

Proceedings

# Anti- and hyper- nuclei production at the LHC with ALICE<sup>†</sup>

Luca Barioglio<sup>1</sup> on behalf of the ALICE Collaboration

<sup>1</sup> INFN and Università degli Studi di Torino

† Presented at Hot Quarks 2018 - Workshop for young scientists on the physics of ultrarelativistic nucleus-nucleus collisions, Texel, The Netherlands, September 7-14 2018

Version December 11, 2018 submitted to Proceedings

**Abstract:** At the Large Hadron Collider (LHC) a significant production of (anti-)(hyper-)nuclei is observed in proton-proton (pp), proton-lead (p-Pb) and lead-lead (Pb-Pb) collisions. The measurement of the production yields of light (anti-)nuclei is extremely important to provide insight into the production mechanisms of nuclear matter, which is still an open question in high energy physics. The outstanding particle identification (PID) capabilities of the ALICE detectors allow the identification of rarely produced particles such as deuterons, <sup>3</sup>He and their antiparticles. From the production spectra measured for light (anti-)nuclei with ALICE, the key observables of the production mechanisms (antimatter/matter ratio, coalescence parameter, nuclei/protons ratio) are computed and compared with the available theoretical models. Another open question is the determination of the hypertriton lifetime: published experimental values show a lifetime shorter than the expected one, which should be close to that of the free  $\Lambda$  hyperon. Thanks to the high-resolution track reconstruction capabilities of the ALICE experiment, it has been possible to determine the hypertriton lifetime at the highest Pb-Pb collisions energy with the highest precision ever reached.

**Keywords:** nuclei, antinuclei, hypertriton lifetime

## 1. Introduction

At the LHC, (anti-)nuclei are abundantly produced in different collision systems and at different energies. Since light nuclei are characterised by a low binding energy ( $E_B \sim 2$  MeV) compared to the temperature of the chemical freeze-out, which is the phase when the abundances of the particle species are fixed ( $T_{ch} \sim 160$  MeV), the study of the nuclear (anti-)matter production mechanisms is crucial to understand how these loosely bound objects can be produced in such extreme conditions.

The study of the production mechanisms is carried out comparing the experimental results with the predictions of the available phenomenological models, namely the statistical-thermal [1] and the coalescence [2] models. According to the statistical thermal model, (anti-)nuclei are produced at the chemical freeze-out in statistical equilibrium, as well as all the other hadrons. On the other hand, in the coalescent picture, nucleons that are close to each other in the phase space after the thermal freeze-out can merge and form a nucleus via coalescence.

At the LHC energies not only (anti-)nuclei, but also (anti-)hypernuclei are produced. In particular, the ALICE experiment measured the production of  ${}^3_{\Lambda}\text{H}$  (hypertriton) in Pb-Pb collisions. A hypernucleus is a nucleus that contains at least one hyperon in addition to the nucleons and the hypertriton is the lightest hypernucleus, consisting of a bound state of a neutron, a proton and a  $\Lambda$  hyperon. The measurement of the hypertriton lifetime is extremely important because it can give an insight of the internal structure of this hypernucleus and because the latest measurements showed a slight disagreement with the theoretical predictions [3–5], which are close to the free  $\Lambda$  lifetime. This

34 disagreement is known as the *hypertriton lifetime puzzle*. These analyses are based on data collected by  
 35 ALICE and the description of the detectors can be found in [6].

## 36 2. (Anti-)nuclei production

37 The ALICE experiment has observed the production of nuclei in different collision systems and at  
 38 different energies. In particular, the transverse momentum spectra have been measured for deuterons  
 39 and  $^3\text{H}$  in pp collisions at  $\sqrt{s} = 7$  TeV, in p-Pb collisions at  $\sqrt{s_{NN}} = 5$  TeV and in Pb-Pb collisions at  
 40  $\sqrt{s_{NN}} = 2.76$  TeV [7]. For deuterons, the production spectra have also been measured in pp collisions  
 41 at  $\sqrt{s} = 13$  TeV. The spectra have been measured both for nuclei and antinuclei. The ratio between  
 42 the spectra of antinuclei and nuclei is important to understand whether there is a difference in the  
 43 production of matter and antimatter. The ratios have been evaluated both for deuterons and  $^3\text{He}$   
 44 for all the measurements aforementioned and they are always compatible with the unity within the  
 45 uncertainties. An example of the ratio between the spectra of antideuterons and deuterons is reported  
 46 in in Figure 1. The results are obtained from pp collisions at  $\sqrt{s} = 13$  TeV. The ratios are presented for  
 47 different multiplicity classes, going from the highest (I) to the lowest (X) multiplicity.

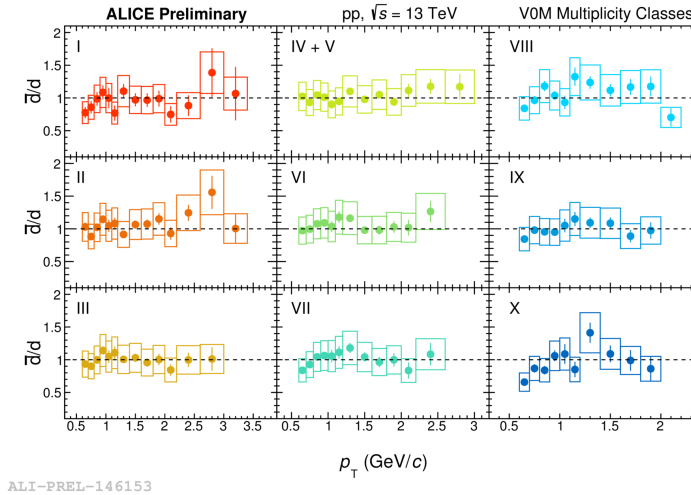


Figure 1. Ratio between the spectra of antideuterons and deuterons.

48 By comparing the  $p_T$  spectra of nuclei and protons, two important observables can be computed:  
 49 the coalescence parameter  $B_A$  and the ratio between the yields of nuclei and protons. The coalescence  
 50 parameter is a quantity related to the probability of forming a nucleus via coalescence and it is defined  
 51 as:

$$B_A(p_T^p) = \frac{\frac{1}{2\pi p_T^A} \frac{d^2 N_A}{dp_T^A dy}}{\left(\frac{1}{2\pi p_T^p} \frac{d^2 N_p}{dp_T^p dy}\right)^A}, \quad \text{with } p_T^p = p_T^A / A \quad (1)$$

52 where  $A$  is the mass number of the nucleus,  $p_T^p$  and  $p_T^A$  are the proton and the nucleus transverse  
 53 momentum respectively. Here the case of deuterons is discussed and the latest ALICE results of the  $B_2$   
 54 and the  $d/p$  are shown.

55 The  $B_2$  as a function of  $p_T$  is computed for all the collision systems and energies listed above. In  
 56 order to compare the  $B_2$  in the different collision systems, the value obtained for each of these at  
 57  $p_T/A = 0.75$  GeV/c is plotted as a function of the event multiplicity (Figure 2). This particular  $p_T$   
 58 bin ( $[0.7; 0.8]$  GeV/c) has been chosen because it is common between all the analyses. However, the  
 59 evolution of the  $B_2$  with the multiplicity is very similar in the other  $p_T$  bins. The coalescence parameter

60 evolves smoothly with the event multiplicity, without any discontinuity passing from a colliding  
 61 system to another, suggesting a common production mechanism between small and large systems that  
 62 depends only on the event multiplicity and consequently on the size of the collision system. Two kinds  
 63 of regimes can be distinguished. At low multiplicity, the coalescence parameter is slightly decreasing,  
 64 while at high multiplicity it decreases more quickly. A possible explanation is that at low multiplicities  
 65 the system size is comparable with the deuteron size, while increasing the multiplicity the system size  
 66 becomes larger and larger and the probability to form a nucleus via coalescence becomes smaller.

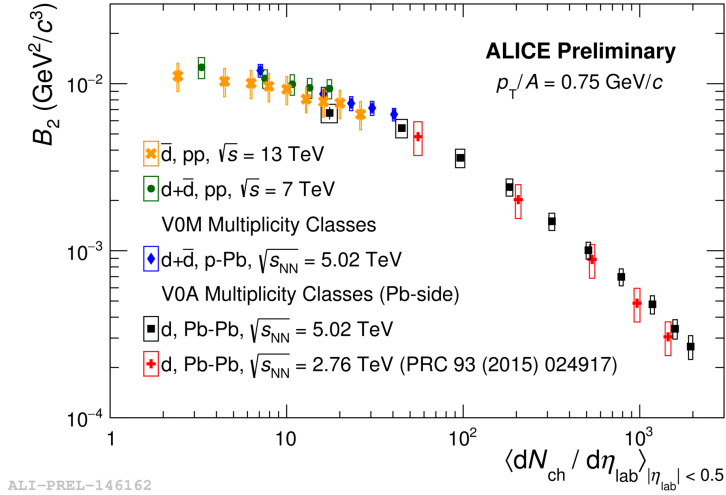


Figure 2. Coalescence parameter  $B_2$  at  $p_T/A = 0.75$  GeV/ $c$  as a function of multiplicity.

67 A similar behaviour is seen for the ratio between the  $p_T$ -integrated yields of deuterons and protons  
 68 as a function of multiplicity (Figure 3). The deuteron and proton spectra are fitted with a Levy-Tsallis  
 69 distribution [8] in pp collisions and with a Blast-Wave function [9] in p-Pb and Pb-Pb collisions, in  
 70 order to extrapolate the yields in the unmeasured regions at low and high  $p_T$  and integrate over the  
 71 full  $p_T$  range. The ratio evolves smoothly with the multiplicity and it shows no discontinuity between  
 72 different collision systems and different energies. Generally, for small systems the ratio is increasing,  
 73 in agreement with the predictions of the coalescence model, while for larger systems such as Pb-Pb the  
 74 ratio is flat, in agreement with the predictions of the thermal model.

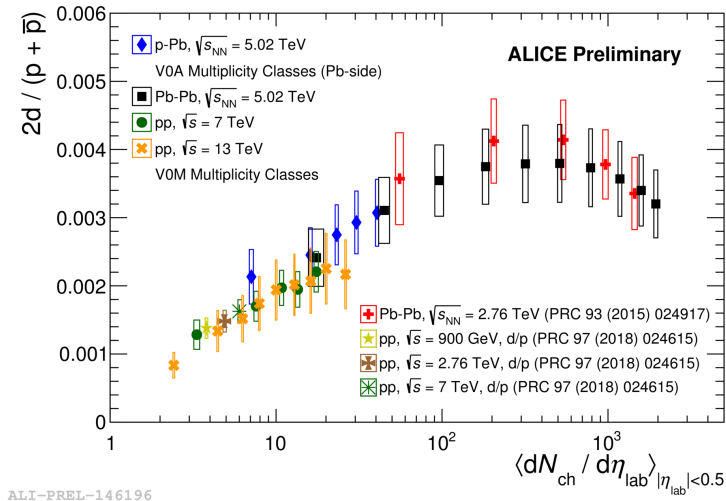
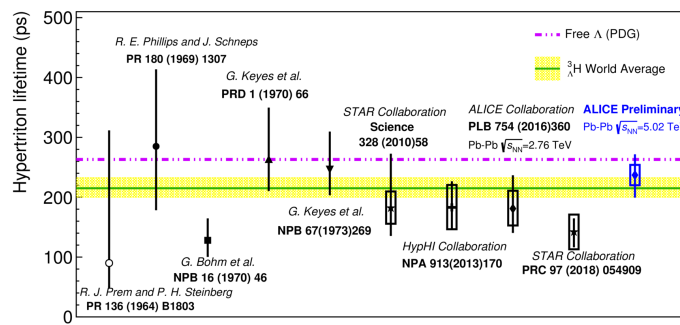


Figure 3. Ratio between the deuteron and proton yields as a function of the event multiplicity.

75 In conclusion, the thermal model provides a better description of the experimental data in large  
 76 systems, while the coalescence model works well for small systems. However, the smooth evolution of  
 77 the  $B_2$  and the  $d/p$  suggests a system size dependent common production mechanism..

### 78 3. The hypertriton lifetime

79 The hypertriton is characterised by a low  $\Lambda$  separation energy ( $E_B = 130$  keV) and for this reason  
 80 the lifetime is expected to be close to that of the free  $\Lambda$  [3–5]. Over time, several measurements have  
 81 been carried out. They can be grouped according to the experimental techniques: visualising and  
 82 ion-beam based. The former, like bubble chambers and emulsions, give results compatible within  $1\sigma$   
 83 with the free  $\Lambda$  lifetime, but these measurements have large uncertainties. The latter, relying on large  
 84 data samples, have lower uncertainties and are slightly but systematically below the predicted value.  
 85 The ALICE collaboration measured the hypertriton lifetime via the two-body mesonic decay channel  
 86  ${}^3_{\Lambda}H \rightarrow {}^3He + \pi$  in the Pb-Pb data sample at  $\sqrt{s_{NN}} = 5$  TeV. The result is the most precise ever  
 87 obtained and it is compatible within  $1\sigma$  both with the world average and the free  $\Lambda$  lifetime. Recently  
 88 the STAR collaboration published a lower value, but compatible within  $2\sigma$  with the ALICE result.  
 89 More precise measurements will be possible with the large data samples that have been collected in  
 90 the 2018 Pb-Pb acquisition and that will be collected during Run 3.



ALI-DER-161043

**Figure 4.** Collection plot of hypertriton lifetime measurements. In blue the latest ALICE results, which is the most precise measurement ever obtained.

### 91 References

- 92 1. A. Andronic, P. Braun-Munzinger, J. Stachel and H. Stocker, *Phys. Lett. B* **697** (2011) 203  
 93 doi:10.1016/j.physletb.2011.01.053 [arXiv:1010.2995 [nucl-th]].
- 94 2. J. I. Kapusta, *Phys. Rev. C* **21** (1980) 1301. doi:10.1103/PhysRevC.21.1301
- 95 3. M. Rayet and R. H. Dalitz, *Nuovo Cim. A* **46** (1966) 786.
- 96 4. J. G. Congleton, *J. Phys. G* **18** (1992) 339. doi:10.1088/0954-3899/18/2/015
- 97 5. H. Kamada, J. Golak, K. Miyagawa, H. Witala and W. Gloeckle, *Phys. Rev. C* **57** (1998) 1595  
 98 doi:10.1103/PhysRevC.57.1595 [nucl-th/9709035].
- 99 6. B. B. Abelev *et al.* [ALICE Collaboration], *Int. J. Mod. Phys. A* **29** (2014) 1430044  
 100 doi:10.1142/S0217751X14300440 [arXiv:1402.4476 [nucl-ex]].
- 101 7. J. Adam *et al.* [ALICE Collaboration], *Phys. Rev. C* **93** (2016) no.2, 024917 doi:10.1103/PhysRevC.93.024917  
 102 [arXiv:1506.08951 [nucl-ex]].
- 103 8. C. Tsallis, *J. Statist. Phys.* **52** (1988) 479. doi:10.1007/BF01016429
- 104 9. E. Schnedermann, J. Sollfrank and U. W. Heinz, *Phys. Rev. C* **48** (1993) 2462 doi:10.1103/PhysRevC.48.2462  
 105 [nucl-th/9307020].

106       © 2018 by the authors. Submitted to *Proceedings* for possible open access publication  
107 under the terms and conditions of the Creative Commons Attribution (CC BY) license  
108 (<http://creativecommons.org/licenses/by/4.0/>).